JOURNAL OF APPLIED ELECTROCHEMISTRY **26** (1996) 471–479

Modelling mass transfer entrance lengths in turbulent pipe-flow with applications to small cathodes for measuring local mass transfer rates

Y. WANG*, J. POSTLETHWAITE*† and D. J. BERGSTROM‡

Department of Chemical Engineering, Department of Mechanical Engineering‡, University of Saskatchewan, Saskatoon, Saskatchewan, S7N 5C9, Canada*

Received 28 February 1995; revised 20 September 1995

Pipe-wall mass transfer, in the developing concentration boundary layer region, under fully developed hydrodynamic conditions is simulated with a low-Reynolds number, k–ϵ, eddy viscosity turbulence model. The predictions are in good agreement with the electrochemical measurements of Berger and Hau, in the range $Re = 10^4$ to 10^5, for $Sc = 2244$, and of Son and Hanratty, in the range $Re = 1 \times 10^4$–5×10^4, for $Sc = 2400$, in both the developing boundary layer region and the fully developed region. The application of small cathodes embedded in a larger active cathode to measure local mass transfer rates is also simulated. The size of the electrode and the thickness of the electrical insulation around the small electrode give rise to errors that increase as the insulation thickness increases and the electrode size decreases.

List of symbols

$C_\mu, C_{\epsilon 1}, C_{\epsilon 2}$	turbulence model constants
f_μ, f_1, f_2	turbulence model functions
c	species concentration
d	diameter of straight pipe
D	molecular diffusion coefficient
k	kinetic energy of turbulence, $\frac{1}{2}\overline{u_i u_i}$
K	local mass transfer coefficient
$\langle K \rangle$	mean mass transfer coefficient
L	distance from the mass transfer entrance
P	pressure
P_k	production of turbulence
r	radial coordinate
Re	Reynolds number
Re_T	turbulence Reynolds number, $\rho k^2/\mu\epsilon$
S	source term
Sc	Schmidt number, ν/D
St_d	local Stanton number, K/U_b
$\langle St_d \rangle$	mean Stanton number, $\langle K \rangle/U_b$
u, v	components of the fluctuation velocity vector
U, V	components of mean velocity vector
U_b	bulk flow velocity
u_τ	friction velocity, $(\tau_w/\rho)^{1/2}$
u_ϵ	Kolmogorov velocity, $(\nu\epsilon)^{1/4}$
x	axial coordinate
y	distance from the wall
K^+	dimensionless local mass transfer coefficient, K/u_τ
$\langle K^+ \rangle$	dimensionless mean mass transfer coefficient, $\langle K \rangle/u_\tau$
L^+	dimensionless distance from the entrance, Lu_τ/ν
y^+	dimensionless distance from the wall, yu_τ/ν
y^*	dimensionless distance from the wall, yu_ϵ/ν
δy	distance of nearest node from wall surface

Greek symbols

Γ	diffusion coefficient
ϵ	dissipation of kinetic energy of turbulence, $2\mu/\rho\overline{s_{ij}s_{ij}}$
μ	dynamic viscosity
μ_t	turbulent viscosity
ρ	fluid density
$\sigma_k, \sigma_\epsilon, \sigma_m$	turbulent Prandtl–Schmidt numbers
Φ	general variable

Subscripts

eff	effective value (molecular + turbulent)
k	kinetic energy of turbulence
t	turbulent value
b	bulk value
w	wall surface
f	nearest node from wall surface
∞	fully developed value

† Author to whom correspondence should be addressed.

0021-891X

1. Introduction

Erosion–corrosion in aqueous solutions is often mass transfer controlled [1, 2]. The mass transfer control can occur at small patches on a pipe wall, where a protective corrosion product film has been disrupted, and involve a region of developing concentration boundary layer [3–5]. In the present study, a low Reynolds number k–ϵ eddy viscosity model is used to predict wall mass transfer rates in the region of developing concentration boundary layer, as part of an ongoing program for the development of numerical models for the simulation of erosion–corrosion [6–8].

Entrance length effects, relating to the discontinuity caused by the electrical insulation, on small local cathodes located in a large active cathode are also investigated, since in principle the latter small local cathodes offer a means for experimentally determining local mass transfer rates in the entrance length region.

A number of experimental studies of mass transfer to the pipe wall both in the developing concentration boundary layer and in the fully developed regions in turbulent flow have been published [9–14]. Linton and Sherwood [9], and Meyerink and Friedlander [14] have measured the dissolution rate of a soluble section of a pipe in a developing concentration boundary layer and fully developed regions. Son and Hanratty [11] and Berger and Hau [13] investigated the mass transfer behaviour in the entrance region, using electrochemical limiting diffusion current techniques to measure mean mass transfer coefficients for electrodes of various lengths.

Schutz [15] measured local mass transfer coefficients in the mass transfer entrance region, using small local cathodes fitted into a much larger active cathode. Sprague [16] measured local mass transfer coefficients in bends. Deslouis [17, 18] conducted local mass transfer rate measurements, using microelectrodes installed on a rotating circular disk. In these studies, the small local electrodes were electrically insulated from the cathode by epoxy resin of various thickness that would cause a discontinuity in the mass transfer boundary layer at the surface and result in the enhancement of mass transfer rate at the leading edge of the local electrode.

Furuta *et al.* [19] have investigated theoretically and experimentally the effect of insulation of a circular electrode on the accuracy of local mass transfer measurement under fully developed flow. Wein and Wichterle [20] analysed theoretically the effect of insulating thickness on the current distribution for three segment probes in laminar flow. In the above theoretical studies, some simplifications have been made (e.g., effect of turbulence on mass flux neglected [19]). In this study, the LRN, k–ϵ turbulence model was used to simulate the effect of insulation thickness on the mass transfer measurement of small local electrode.

2. Turbulence model

2.1. *Origin*

The turbulence model used in present study is based on the standard single phase k–ϵ model of turbulence proposed by Launder and Spalding [21]. The eddy viscosity concept used in the k–ϵ model, proposed by Boussinesq, assumes that the effect of turbulence on the mean flow can be taken into account through viscosity [22]. The turbulent viscosity, μ_t, is determined from the kinetic energy of turbulence, k, and its dissipation rate, ϵ:

$$\mu_t = C_\mu f_\mu \rho \frac{k^2}{\epsilon} \tag{1}$$

The mass transfer is modelled by simultaneously solving the conservation equations for mass, momentum, kinetic energy of turbulence and its dissipation as well as species concentration which can be written in the following form (in 2D cylindrical coordinates):

$$\frac{\partial}{\partial x}(\rho U \Phi) + \frac{1}{r}\frac{\partial}{\partial r}(r\rho V \Phi) = \frac{\partial}{\partial x}\left(\Gamma_\Phi \frac{\partial \Phi}{\partial x}\right) + \frac{1}{r}\frac{\partial}{\partial r}\left(r\Gamma_\Phi \frac{\partial \Phi}{\partial r}\right) + S_\Phi \tag{2}$$

where $\Phi = U, V, k, \epsilon, c, \ldots$.

Table 1. Conservation equations

Conservation of	Φ	Γ_Φ	S_Φ
Mass	1	0	0
Axial momentum	U	μ_{eff}	$\frac{\partial}{\partial x}\left(\mu_{\text{eff}}\frac{\partial U}{\partial x}\right)+\frac{1}{r}\frac{\partial}{\partial r}\left(r\mu_{\text{eff}}\frac{\partial V}{\partial x}\right)-\frac{\partial P}{\partial x}$
Radial momentum	V	μ_{eff}	$\frac{\partial}{\partial x}\left(\mu_{\text{eff}}\frac{\partial U}{\partial r}\right)+\frac{1}{r}\frac{\partial}{\partial r}\left(r\mu_{\text{eff}}\frac{\partial V}{\partial r}\right)-2\mu_{\text{eff}}\frac{V}{r^2}-\frac{\partial P}{\partial r}$
Turbulent kinetic energy	k	$\mu+\frac{\mu_t}{\sigma_k}$	$P_k-\rho\epsilon$
Turbulent dissipation rate	ϵ	$\mu+\frac{\mu_t}{\sigma_\epsilon}$	$\frac{\epsilon}{k}(C_{\epsilon 1}f_1 P_k - C_{\epsilon 2}f_2\rho\epsilon)$
Species	c	ρD_{eff}	0

$$P_k = \mu_t\left\{2\left[\left(\frac{\partial U}{\partial x}\right)^2+\left(\frac{\partial V}{\partial r}\right)^2+\left(\frac{V}{r}\right)^2\right]+\left(\frac{\partial U}{\partial r}+\frac{\partial V}{\partial x}\right)^2\right\}$$

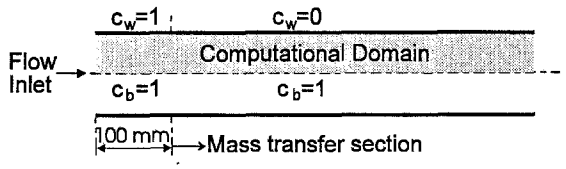

Fig. 1. Computational domain. Fully developed flow at inlet. Mass transfer section commences at 100 mm. Concentrations c_w and c_b are normalized. Pipe diameter: 54.8 mm, 25.4 mm and 40 mm.

The general diffusion coefficients, Γ_Φ, and the source terms, S_Φ, are given in Table 1.

The effective viscosity, μ_{eff}, and diffusivity, D_{eff}, are given by

$$\underbrace{\mu_{\text{eff}}}_{\text{effective}} = \underbrace{\mu}_{\text{molecular}} + \underbrace{\mu_t}_{\text{turbulent}} \tag{3}$$

$$\underbrace{D_{\text{eff}}}_{\text{effective}} = \underbrace{\frac{\mu}{\rho S_c}}_{\text{molecular}} + \underbrace{\frac{\mu_t}{\rho \sigma_m}}_{\text{turbulent}} \tag{4}$$

where the turbulent Prandtl Schmidt number σ_m is set at 0.9 [23].

2.2. *Boundary conditions*

The conservation equations are elliptic partial differential equations that require the boundary conditions for all variables on all boundaries of the flow domain: inlet, exit, wall and symmetry axis. At the inlet, the mean and fluctuating velocities can be taken from established values for fully developed flow, while zero gradients can be set at the axis and outlet. For mass transfer, the normalized species concentrations at the wall and the axis are given in Fig. 1.

Two basic approaches in the near-wall region have been widely used: the universal wall function (WF) model and the low Reynolds number (LRN) model. The WF approach bridges over the near-wall region with a universal logarithmic velocity profile. However, the first computation node is typically located so that $30 < y^+ < 150$, which misses important features of the mass transfer sublayer, the thickness of which is an order of magnitude smaller than the thickness of the hydrodynamic viscous sublayer for aqueous flow at high Schmidt numbers [24]. This explains why the LRN approach, which enables the application of the k–ϵ model very close to the wall, should be used in the case of modelling mass transfer in turbulent aqueous flow.

Many low Reynolds number k–ϵ models have been proposed in the past two decades [25–27], among which the model proposed by Nagano and Tagawa [27] (NT) can reproduce the near-wall limiting behaviour and provides accurate predictions for attached turbulent flows, such as pipe flow, that are required for accurate prediction of wall mass transfer. More recently, a modified version of the NT model has been proposed by Abe, Kondoh and Nagano (AKN) [28], in which the Kolmogorov velocity scale $u_\epsilon \equiv (\nu\epsilon)^{1/4}$, instead of the friction velocity u_τ, is used to account for the near-wall and low Reynolds number effects in both attached and separated flows.

Table 2. Constants and functions in both NT and AKN models

NT model

c_μ	$c_{\epsilon 1}$	$c_{\epsilon 2}$	σ_k	σ_ϵ
0.09	1.45	1.9	1.4	1.3

$$f_\mu = \left[1 - \exp\left(-\frac{y^+}{26}\right)\right]^2 \left[1 + \frac{4.1}{R_t^{0.75}}\right]$$

$$f_1 = 1$$

$$f_2 = \left[1 - 0.3\exp\left(-\left(\frac{R_t}{6.5}\right)^2\right)\right]\left[1 - \exp\left(-\frac{y^+}{6}\right)\right]^2$$

AKN model

c_μ	$c_{\epsilon 1}$	$c_{\epsilon 2}$	σ_k	σ_ϵ
0.09	1.5	1.9	1.4	1.4

$$f_\mu = \left[1 - \exp\left(-\frac{y^*}{14}\right)\right]^2 \left[1 + \frac{5}{R_t^{0.75}}\exp\left\{-\left(\frac{R_t}{200}\right)^2\right\}\right]$$

$$f_1 = 1$$

$$f_2 = \left[1 - 0.3\exp\left(-\left(\frac{R_t}{6.5}\right)^2\right)\right]\left[1 - \exp\left(-\frac{y^*}{3.1}\right)\right]^2$$

In the present study, the two models are compared, and the AKN model is selected for subsequent calculations. The turbulence model functions f_μ, f_1 and f_2 as well as the model constants are given in Table 2.

At the wall, we set $k = 0$. The strict boundary condition for ϵ is $\epsilon = \nu(\partial^2 k/\partial y^2)|_{\text{wall}}$, which is derived from the differential equation of kinetic energy of turbulence. However this type of boundary condition may lead to instabilities during the iterative calculations because the second-order derivative cannot be guaranteed to provide the positive value. In order to avoid using the second order derivative at the boundary, $\epsilon = \nu(2k_f/(\delta y)^2)$ was used in this study as boundary condition for ϵ. The validity of the equation can be shown by expanding k_f about y in the Taylor series

$$k_f = k_w + \left.\frac{\partial k}{\partial y}\right|_w (\delta y) + \frac{1}{2}\left.\frac{\partial^2 k}{\partial y^2}\right|_w (\delta y)^2 + O(\delta y)^3 \tag{5}$$

Since $k_w = 0$ and $(\partial k/\partial y)|_w = 0$ based on the definition of k and continuity equation, following equation can be obtained:

$$\epsilon_w = \nu\left.\frac{\partial^2 k}{\partial y^2}\right|_w = \nu\frac{2k_f}{(\delta y)^2} \quad \text{for } \delta y \to 0 \tag{6}$$

2.3. *Numerical solution*

The conservation equations were solved numerically using the SIMPLE (semi-implicit method for pressure linked equation) algorithm. The SIMPLE procedure has been described in detail by Patankar and Spalding [29, 30]. The main idea is to introduce the pressure into the continuity equation and in that way link it with the momentum equation. Non-uniform staggered grids (91 × 40) were used with the majority of nodes clustered in the near-wall region and mass transfer entrance region. The first near-wall node was placed at $y = 0.5 \sim 1\ \mu$m so that $y^+ \leq 0.1$, and

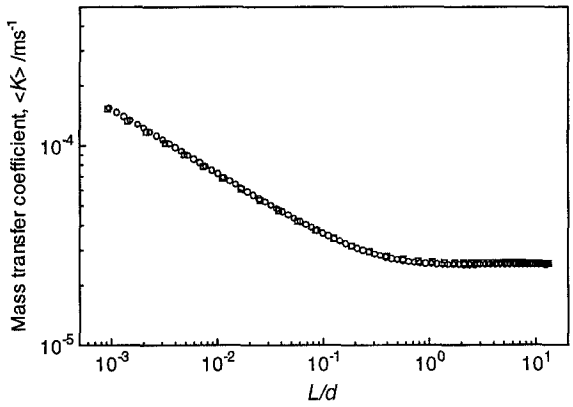

Fig. 2. Evaluation of grid dependence on computational results. Grid systems: (□) 91 × 40; (○) 121 × 60. $Re = 63\,200$; $d = 54.8$ mm.

the first node close to the mass transfer entrance was placed at $x = 1\,\mu$m. To account for the rapid change of concentration profile caused by insulating layer of epoxy resin in the near wall region in the case of small electrodes embedded in large active electrodes, a finer grid system, 201 × 60, was used with the first near-wall node placed at $y = 0.2\,\mu$m. The transport equations were solved using an iterative solution procedure until the total normalized residual for each variable was reduced to the value of 0.001.

2.4. *Calculation of mass transfer coefficients*

The application of the low Reynolds number model enables the calculation of species concentration profiles all the way to the wall. If the first node is placed within the diffusion controlled mass transfer sublayer, the local mass transfer coefficient, K, can be calculated from the following equation:

$$K = \frac{D(c_f - c_w)}{(\delta y)(c_b - c_w)} \tag{7}$$

The mean mass transfer coefficients are estimated by integrating local values over a certain length of mass transfer section.

Two grid systems (91 × 40 and 121 × 60) have been used to evaluate the grid dependence of the computational results. The comparison is shown in Fig. 2 where it is seen that the grid system (91 × 40) is sufficiently accurate to calculate the mass transfer coefficient profile in mass transfer entrance region when $L/d > 10^{-3}$. The results from two grid systems with different distance of first nodes from wall (Fig. 3) indicate that the concentration profile is approximately linear within diffusion controlled boundary layer ($y^+ < 0.1$) and Equation 7 is suitable to estimate the first derivative of the concentration profile.

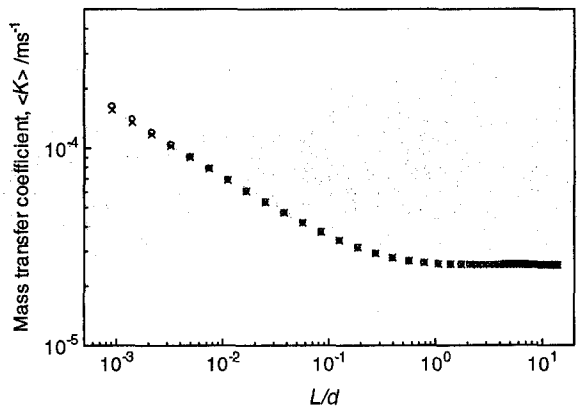

Fig. 3. Effect of the distance of first node from the wall on the evaluation of mass transfer coefficients. First node from wall: (×) 0.5 μm; (○) 1.0 μm. $Re = 63\,200$; $d = 54.8$ mm.

3. Results and discussions

3.1. *Entrance length*

The experimental studies of Berger and Hau [13] and Son and Hanratty [11], of mass transfer in the developing concentration boundary layer region were numerically simulated. The Berger and Hau study included experiments with nine mass transfer sections with an internal diameter of 54.8 mm and varying lengths from 0.008 to 9.12 pipe-diameters, with Reynolds numbers from $1.29 \sim 13.5 \times 10^4$ and a Schmidt number of 2244. In the Son and Hanratty experiments ten test sections with internal diameter of 25.4 mm and varying lengths from 0.0177 to 4.31 pipe-diameters, were used, with Reynolds numbers from 4000 to 62 000 and a Schmidt number of 2400.

The predicted (NT and AKN models) and measured (Berger and Hau) wall-mass transfer rates, expressed in terms of mean Stanton numbers, in the developing concentration boundary layer and fully developed regions are compared in Fig. 4 for a Reynolds number of 63 200. Since the measured mass transfer rates are the mean value for each mass transfer test section, the numerically predicted local mass transfer rates have been averaged over each mass transfer section. The Stanton number in the fully developed region where,

$$St_d = 0.0165\, Re^{-0.14} Sc^{-0.67} \tag{8}$$

given by Berger and Hau [13] is also shown. In the developing concentration boundary layer region the predictions with both, NT and AKN, LRN models are in good agreement with the experimental

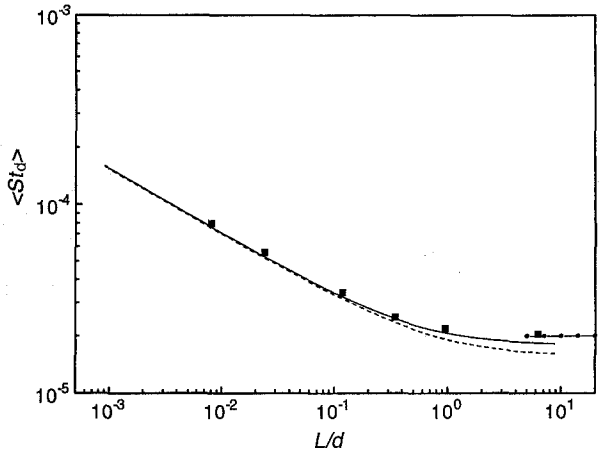

Fig. 4. Variation of mean Stanton number with L/d; $Re = 63\,200$, $d = 54.8$ mm, $Sc = 2244$. Key: (——) AKN model [28]; (– – –) NT model [27]; (■) experiment [13]; (–●–) correlation [13] for fully developed mass transfer.

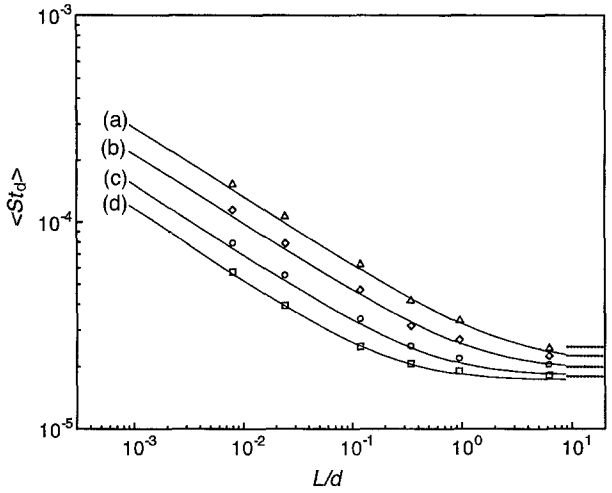

Fig. 5. Variation of mean Stanton number with L/d; $d = 54.8$ mm, $Sc = 2244$. Key: (△, ◇, ○, □) experiment [13]; (——) predictions; (•••••) correlation [13]. *Re*: (△) 12 900; (◇) 26 000; (○) 63 200 and (□) 135 000.

measurements. In the fully developed region, both models give predictions that are lower than the measurements, with the relative error −18.5% for the NT model and −7% for the AKN model. Therefore, the AKN, LRN model was used for the remainder of the study.

The variation of the predicted and measured (Berger and Hau) mean Stanton numbers with L/d in the region of developing concentration boundary layer, for four different Reynolds numbers, are shown in Fig. 5, as well as the Stanton numbers in the fully developed region. The predictions are in excellent agreement with the measurements for all four Reynolds numbers in the region of developing

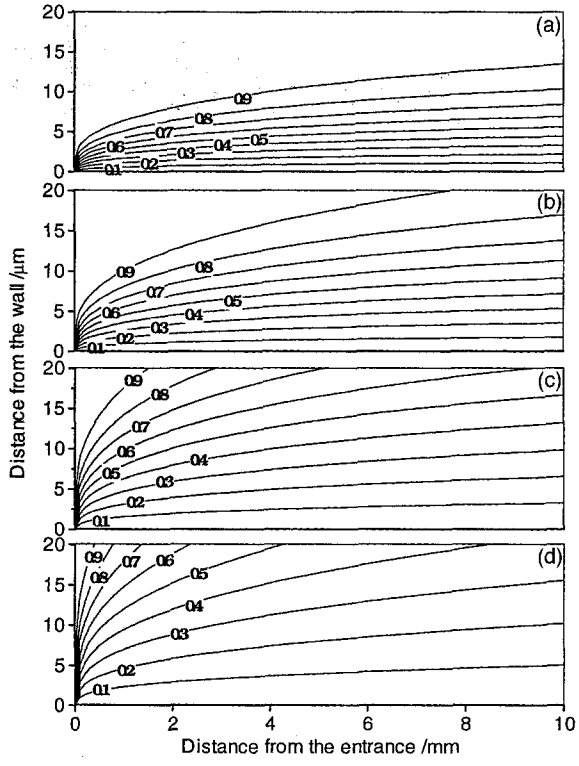

Fig. 6. Normalized concentration distribution of $Fe(CN)_6^{3-}$ in the developing concentration boundary layer region for four Reynolds numbers. Lines correspond to the normalized concentration contours. *Re*: (a) 135 000; (b) 63 200; (c) 26 000 and (d) 12 900.

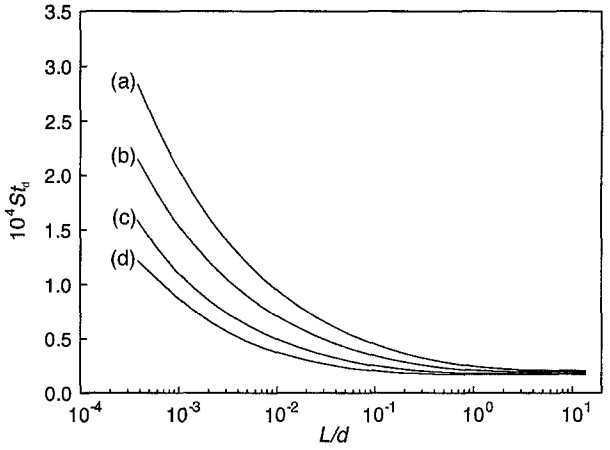

Fig. 7. Variation of local Stanton number with L/d; $d = 54.8$ mm. *Re*: (a) 12 900; (b) 26 000; (c) 63 200 and (d) 135 000.

concentration boundary layer. In the fully developed region, the predicted Stanton numbers are very close to the experimental values.

The normalized simulated concentration distributions of $Fe(CN)_6^{3-}$ for four Reynolds numbers (Berger and Hau) in the mass transfer entrance region (Fig. 6) show the effect of the Reynolds number on the entrance length and on the thickness of the fully developed concentration boundary layer. The variation of local Stanton numbers (calculated from the simulated local mass transfer coefficients) with L/d are shown in Fig. 7. The mass transfer rates approach infinity at the beginning of the mass transfer section. For all Reynolds numbers investigated, the Stanton numbers reach the fully developed values at $L/d \leq 5$. If the entrance length is defined as the distance from the entrance where local Stanton number reaches a value 5% higher than the fully developed value, the entrance length, based on the predictions, was found to vary from $L/d \approx 5$ for $Re = 12\,900$ to $L/d \approx 0.25$ for $Re = 135\,000$ at $Sc = 2244$. If experiments are to be done under conditions where the effect of the entrance length can be neglected and the mean mass transfer coefficients approach the fully developed values then L/d values ≈ 9.7 at $Re = 26\,000$ to $L/d \approx 1.6$ at $Re = 135\,000$, with $Sc = 2244$ are required.

The variation of predicted dimensionless mean mass transfer coefficients, $\langle K^+ \rangle$, with dimensionless distance from the entrance, L^+, are shown in Fig. 8, where they are compared to the results of Son and Hanratty [11]. It is seen that the present numerical predictions are in good agreement with the measurements for four Reynolds numbers in the mass transfer entrance region. In the fully developed region, the predictions are also in good agreement with the measurements with relative error less than 5%. The predictions indicate that the entrance length needed for the local mass transfer coefficient to become fully developed, $K^+ \approx K_\infty^+$, varies from $L^+ \approx 2500$ ($L/d \approx 4.32$) for $Re = 10\,000$ to $L^+ \approx 1700$ ($L/d = 0.58$) for $Re = 55\,100$ at $Sc = 2400$. The entrance length for the mean mass transfer coefficient to approach the fully developed value, $\langle K^+ \rangle \approx K_\infty^+$, varies from $L^+ \approx 1.5 \times 10^4$ ($L/d \approx 12.48$) for $Re = 20\,000$ to $L^+ \approx 1.1 \times 10^4$

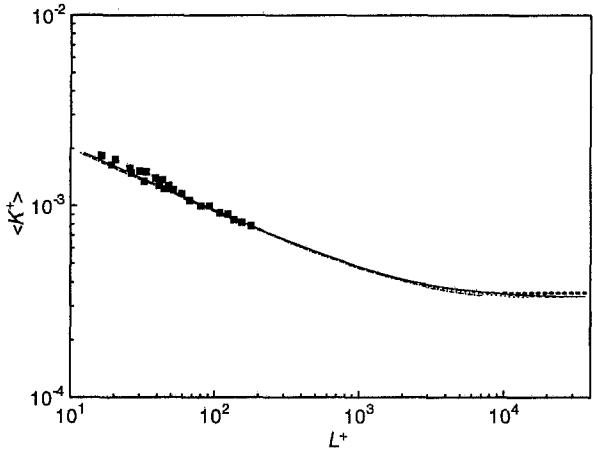

Fig. 8. Variation of dimensionless mass transfer coefficient with L^+; $d = 25.4$ mm. Re: (——) 55 100; (– – –) 40 000; (· · · ·) 20 000; (· – · – · –) 10 000; (■) experiment [11] and (– – –) correlation [11] for fully developed mass transfer. $Re = 8770 \sim 55\,100$; $Sc = 2400$.

($L/d \approx 3.81$) for $Re = 55\,100$. Both predictions for dimensionless entrance lengths are in good agreement with other researchers' experimental results [12, 31, 32].

Figure 9 shows the variation of concentration profile with distance from the entrance in the near-wall region. It is seen that the concentration profile undergoes a rapid change after entering the mass transfer section. An original flat profile changes to one exhibiting a large gradient of concentration near the wall. Finally, a fully developed concentration profile is reached if the mass transfer section is long enough.

The predicted momentum and mass transfer transport coefficients μ_{eff} and D_{eff} in the fully developed concentration boundary layer region for $Re = 63\,200$ and $Sc = 2244$ are shown in Fig. 10. Far from the wall ($y \geq 1$ mm), the effective viscosity is about 10 times larger than molecular viscosity, indicating that the flow is dominated by turbulent transport. As the wall is approached, the magnitude of effective viscosity approaches the value of molecular viscosity, indicating that the turbulence is gradually being damped. Consequently, the viscous sublayer with a thickness of $y \approx 60\ \mu$m is formed, in which the flow is controlled by viscous forces. Although very little turbulence is

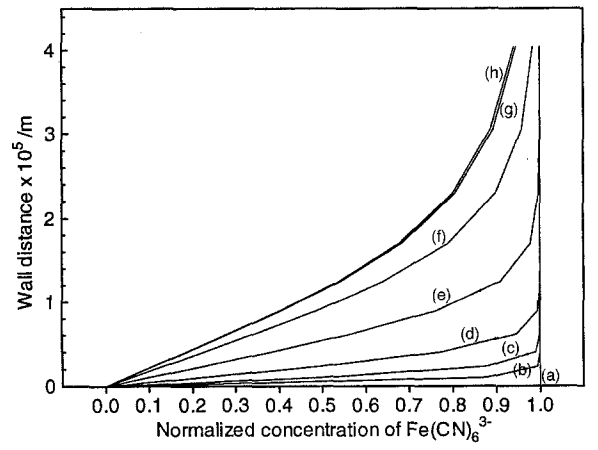

Fig. 9. Change of concentration profile with distance from the entrance in the near wall region; $Re = 63\,200$, $d = 54.8$ mm, $Sc = 2244$. L/d: (a) 0; (b) 1.82×10^{-5}; (c) 2.37×10^{-4}; (d) 2.13×10^{-3}; (e) 2.51×10^{-2}; (f) 1.86×10^{-1}; (g) 1.06 and (h) 6.11.

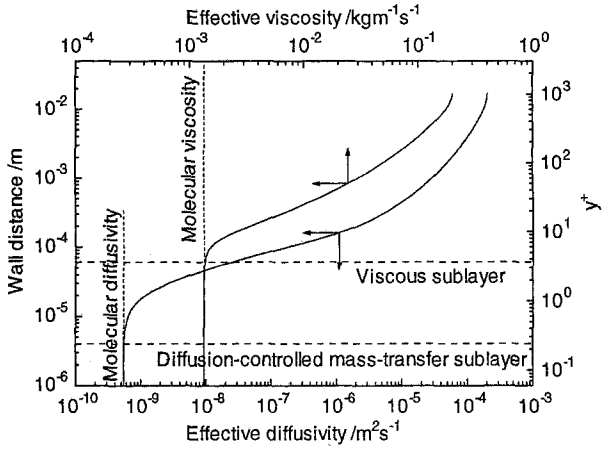

Fig. 10. Variation of transport coefficients with the distance from the wall; $Re = 63\,200$, $Sc = 2244$, $d = 54.8$ mm.

retained at the edge of the viscous sublayer, the effective diffusivity is still about 60 times larger than the molecular diffusivity. This demonstrates that residual turbulence, which has negligible effect on momentum transport, still has considerable effect on mass transfer. This behaviour is to be expected for fluid with a large Schmidt number. The turbulent diffusivity is reduced as the wall is approached, becoming insignificant at about 4 μm from the wall ($y^+ \approx 0.25$) when mass is transported exclusively by molecular diffusion.

3.2. *Small local cathodes*

Schutz [15] used the limiting diffusion current technique to measure local mass transfer rates in the region of the developing concentration boundary layer, in a 40 mm diameter tube. Schutz's experimental study was numerically simulated in order to investigate the potential errors in the application of small electrodes to measure local mass transfer coefficients in mass transfer entrance regions. The turbulence model used is a 2D model and as a first approach short tubular electrodes were used for the numerical simulations. In Schutz's experiment, 18 round local electrodes of 1 to 3 mm diameters were fitted into a large active cathode. The first local electrode was mounted 2 mm from the entrance. The small electrodes were electrically insulated from the large cathode by a 0.1 mm thick layer of epoxy resin.

The simulated profiles of mass transfer coefficient and surface species concentration in the mass transfer entrance region, with a 1 mm long tubular local electrode and 0.1 mm insulation, are shown in Fig. 11. The normalized simulated concentration distributions of $Fe(CN)_6^{3-}$ in the region around the small electrode are shown in Fig. 12. It can be seen from Fig. 11(a) that the largest change in the local mass transfer coefficient occurs in the leading edge region (< 0.2 mm from the entrance). Thus, a much smaller electrode, say 10 μm in diameter with 1 μm insulation, would be needed to discriminate the local mass transfer rate in this region which would impose severe practical difficulties. In the remaining entrance region and

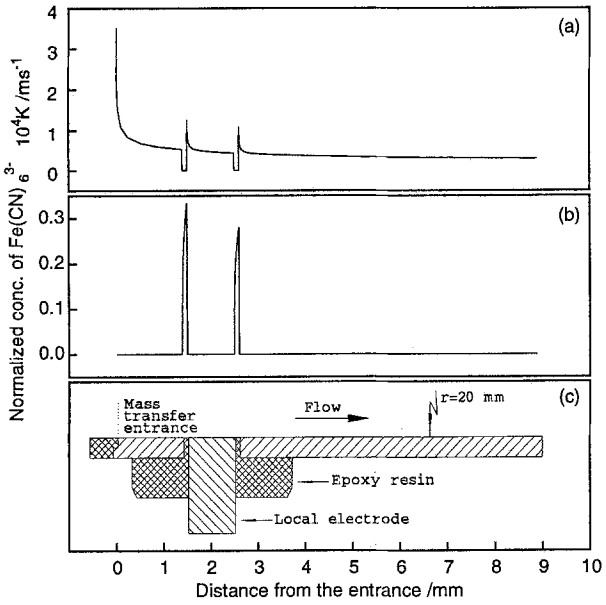

Fig. 11. Variation of the profile of mass transfer coefficient and surface species concentration in the mass transfer entrance region of a 40 mm diameter pipe. A 1 mm long tubular electrode with 0.1 mm insulation is fitted into a large active cathode. $Re = 40\,000$; $Sc = 2170$; $d = 40$ mm.

fully developed region, it is possible to use local electrode to measure local mass transfer coefficients.

We can see from Fig. 11(b) and Fig. 12 that the concentration distributions are disturbed by the insulating junction and the normalized surface species concentration jumps from zero to about 0.35 because there is no mass transfer on the surface of the electrical insulation around the small electrode isolation, which results in the enhancement of the mass transfer coefficient at the leading edge of the local electrode (Fig. 11(a)). Figure 13 shows the effect of electrode size on the measurement error. When a 1 mm wide local electrode with 0.1 mm insulation is used to measure the mass transfer coefficient, the measured value is 7.6% higher than the true value. When a 0.1 mm wide electrode with 0.1 mm insulation is used, the measured value is 45% higher than the true value. The influence of electrical insulation thickness on measurement error caused by the edge effect is shown in Fig. 14, where we can see that thicker insulation creates larger errors.

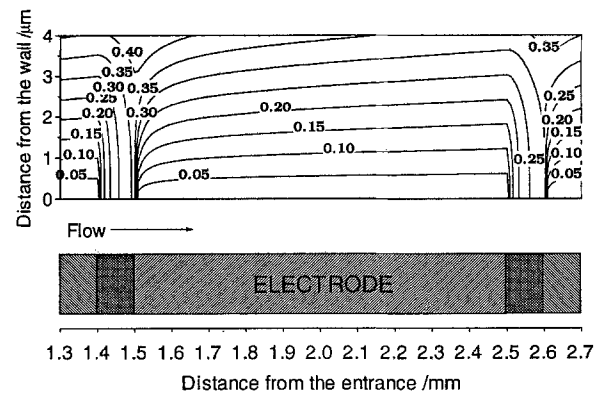

Fig. 12. Normalized concentration distribution of $Fe(CN)_6^{3-}$ in the small electrode region; $Re = 40\,000$, $Sc = 2170$, $d = 40$ mm. Lines correspond to the normalized concentration contours.

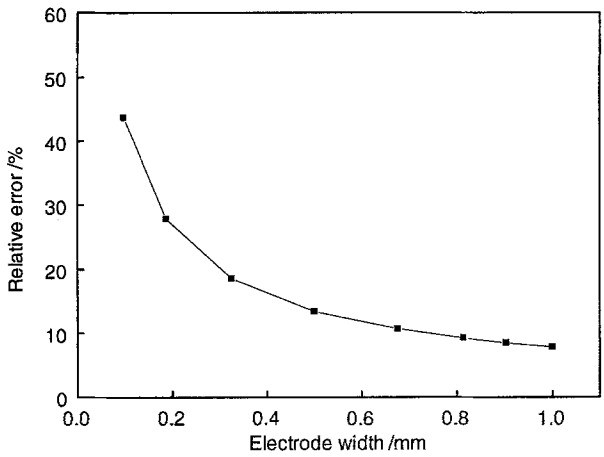

Fig. 13. Effect of local electrode width on measurement error. Insulation thickness: 0.1 mm; $Re = 40\,000$; $Sc = 2170$; $d = 40$ mm.

In the experiments of Deslouis [17, 18], a microelectrode of 80 μm diameter with 10 μm insulation was used to measure local mass transfer coefficients. The present simulation (Fig. 15), with 10 μm insulation in a straight pipe shows that when a local tubular electrode 80 μm long is used the measured value is predicted to be 8.6% higher than the true value, which would be acceptable.

The simulations in Figs 13 and 15 were with a 2D model and the results apply only to the centre line for round local electrodes. And it can be inferred from Figs 13 and 15 that the round local electrodes, which were used by Schutz [15] and Deslouis [17, 18] will produce larger errors than the tubular local electrodes simulated in the present study. Small rectangular local electrodes would give smaller errors than round electrodes with the same surface area.

The above calculations demonstrate the severe practical limitation in measuring local mass transfer coefficients in the leading edge area (< 0.2 mm) of mass transfer entrance regions in pipes. In the remaining region of the entrance section and fully developed concentration region, use of local tubular electrodes would give values close to the true values providing the insulation is sufficiently thin. The application of numerical simulation conditions can assist in assessing the errors during the experimental design stage.

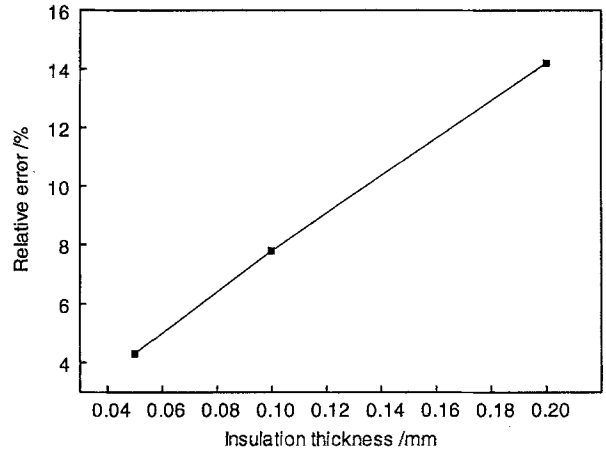

Fig. 14. Effect of insulation thickness on measurement error. Tubular electrode width: 1 mm; $Re = 40\,000$; $Sc = 2170$; $d = 40$ mm.

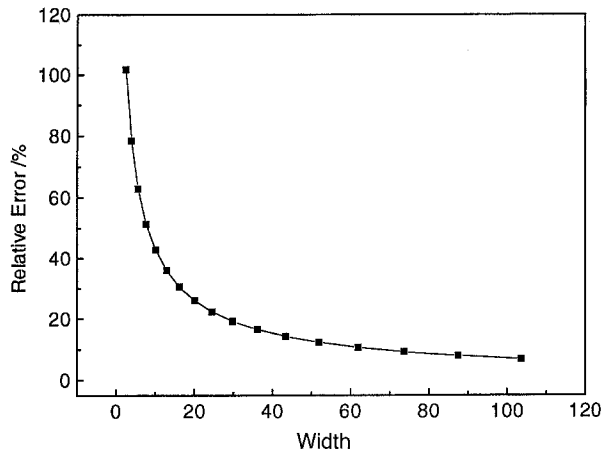

Fig. 15. Effect of local microelectrode width on measurement error. Insulation thickness: 10 μm; $Re = 40\,000$; $Sc = 2170$; $d = 40$ mm.

Three-dimensional simulations would be preferred for small round local electrodes. Unfortunately the simulation time increases quadratically with the number of nodes. Three-dimensional fine mesh requirements for mass transfer simulations at the high Schmidt numbers encountered in aqueous solutions would require considerably more computing power than used in the present study, where the simulation times, with a SPARC station 20–612, are 50 min for the nodes of 91×40 and 224 min for the nodes of 121×60 for $Re = 63\,200$. Three dimensional computational grids would require several orders of magnitude greater simulation times and would also lead to severe memory problem with the size of the arrays generated.

The application of turbulence models to the numerical simulation of mass transfer is relatively recent and there are still questions to be settled regarding the appropriate turbulent Schmidt number [33, 34] to use and the most appropriate turbulence damping model to use near the wall, especially under disturbed flow conditions involving separated flows with recirculation and reattachment [27, 28, 33].

4. Conclusions

(i) Mass transfer in turbulent aqueous flow in a developing concentration boundary layer region in a pipe was simulated using the LRN k–ϵ eddy viscosity model. The predictions were tested against experimental data [11, 13]. The predictions are in good agreement with Berger and Hau's [13] measurements ($Re = 12\,900 \sim 135\,000$, $Sc = 2244$) as well as Son and Hanratty's [11] measurements ($Re = 10\,000 \sim 55\,100$, $Sc = 2400$) in both the developing concentration boundary layer region and the fully developed region.

(ii) The predicted mass transfer entrance length (based on local values of the Stanton number) varies from $L/d \approx 5$ for $Re = 12\,900$ to $L/d \approx 0.25$ for $Re = 135\,000$ at $Sc = 2244$. Mean Stanton numbers are higher than local Stanton numbers in the mass transfer entrance section, and if electrochemical experiments are used to study mass transfer under conditions where the mean K value approaches the fully developed, longer mass transfer sections, from $L/d \approx 9.7$ for $Re = 26\,000$ to $L/d \approx 1.6$ for $Re = 135\,000$, are required.

(iii) There are difficulties in the application of small local electrodes to measure local mass transfer rates caused by edge effects relating to the electrical insulation thickness. The errors increase as the local electrode size is decreased. The use of very small electrodes to study the rapidly changing mass transfer rates at the leading edge (< 0.2 mm) of the mass transfer entrance length, at high Reynolds numbers, would pose severe practical difficulties since electrodes of the order of 10 μm wide with 1 μm insulation would be required. The use of local electrodes of the order of 100 μm wide with 10 μm insulation for studying the balance of the mass transfer entry length is practical.

(iv) Application of low Reynolds number k–ϵ turbulence models to the numerical simulation of mass transfer rates in the developing concentration boundary layer region in pipe flow is a useful complement to experimental studies. Simulation would assist greatly in experimental design and aid in the choice of the size of the local electrodes and insulation thickness. In addition, simulation would give the discrimination necessary at the leading edge of the mass transfer entrance length where there are rapid changes in the rate of mass transfer over distance < 0.2 mm.

References

[1] J. Postlethwaite, M. H. Dobbin and K. Bergevin, *Corrosion* **42** (1986) 514.
[2] U. Lotz, Velocity Effect in Flow Induced Corrosion, *in* 'Flow-Induced Corrosion: Fundamental Studies and Industry Experience' (edited by K. J. Kennelley, R. H. Hausler and D. C. Silverman), NACE, Houston (1991) pp. 8-1 to 8-30.
[3] U. Lotz and E. Heitz, *Werkst. & Korros.* **34** (1983) 454.
[4] B. C. Syrett, *Corrosion* **32** (1976) 242.
[5] J. Postlethwaite, Y. Wang, G. Adamopoulos and S. Nesic, 'Relationship Between Modelled Turbulence Parameters and Corrosion Product Film Stability in Disturbed Single-phase Aqueous Flow', *in* 'Modelling Aqueous Corrosion' (edited by K. R. Trethewey and P. R. Roberge), Kluwer Academic Publishers (1994) pp. 297–316.
[6] S. Nesic and J. Postlethwaite, *Corrosion* **47** (1991) 582.
[7] *Idem, Can. J. Chem. Eng.* **69** (1991) 698.
[8] *Idem, ibid.* **69** (1991) 704.
[9] W. H. Linton, Jr., and T. K. Sherwood, *Chem. Eng. Prog.* **46** (1950) 258.
[10] P. V. Shaw, L. P. Reiss and T. J. Hanratty, *AIChE J.* **9** (1963) 362.
[11] J. S. Son and T. J. Hanratty, *ibid.* **13** (1967) 689.
[12] D. A. Shaw and T. J. Hanratty, *ibid.* **23** (1977) 28.
[13] F. P. Berger and K.-F. F.-L. Hau, *Int. J. Heat Mass Transf.* **20** (1977) 1185.
[14] E. S. C. Meyerink and S. K. Friedlander, *Chem. Eng. Sci.* **17** (1962) 121.
[15] G. Schutz, *Int. J. Heat Mass Transf.* **7** (1964) 1077.
[16] P. J. Sprague, PhD thesis, Exeter University, UK (1984).
[17] C. Deslouis, B. Tribollet and L. Viet, *Electrochim. Acta* **25** (1980) 1027.
[18] C. Deslouis, C. Gabrielli and B. Tribollet, *Physicochemical Hydrodynamics* **2** (1981) 23.
[19] T. Furuta, M. Okazaki and R. Toei, *J. Chem. Eng., Jpn* **7** (1974) 350.
[20] O. Wein and K. Wichterle, *Collec. Czech. Chem. Commun.* **54** (1989) 3198.
[21] B. E. Launder and D. B. Spalding, *Comp. Meth. Appl. Mech. Eng.* **3** (1974) 269.

[22] J. O. Hinze, 'Turbulence', 2nd ed., McGraw-Hill, New York (1975) pp. 23–26.
[23] W. M. Kays and M. E. Crawford, 'Convective Heat and Mass Transfer', McGraw-Hill, New York (1980) pp. 225–229.
[24] V. Levich, 'Physicochemical Hydrodynamics', Prentice-Hall, Englewood Cliffs, NJ (1962) 144–154.
[25] W. P. Jones and B. E. Launder, *Int. J. Heat Mass Transf.* **16** (1973) 1119.
[26] C. K. G. Lam and K. Bremhorst, *ASME J. Fluids Eng.* **103** (1981) 456.
[27] Y. Nagano and M. Tagawa, *ASME J. Fluids Eng.* **112** (1990) 33.
[28] K. Abe, T. Kondoh and Y. Nagano, *Int. J. Heat Mass Transf.* **37** (1994) 139.
[29] S. V. Patankar, 'Numerical Heat Transfer and Fluid Flow', Hemisphere, New York (1980).
[30] S. V. Patankar and D. B. Spalding, *Int. J. Heat Mass Transf.* **15** (1972) 1787.
[31] P. V. Shaw, PhD thesis, University of Illinois, Urbana (1963).
[32] J. S. Son, MS thesis, University of Illinois, Urbana (1965).
[33] S. Nesic, J. Postlethwaite and D. J. Bergstrom, *Int. J. Heat Mass Transf.* **35** (1992) 1977.
[34] D. J Bergstrom, J. W. Gu, S. Nesic and J. Postlethwaite, 'The Application of Low Reynolds Number k–ϵ Models to Mass and Momentum Transport in the Inner and Outer Wall Regions', *in* 'Near-Wall Turbulent Flows', (edited by R. M. C. So, C. G. Speziale and B. E. Launder), Elsevier Science, B.V. (1993) pp. 187–196.